WILEY-VCH

DOI: 10.1002/ ((please add manuscript number))

Article type: Full Paper

The effect of boron and titanium microalloying on the scale formation of AISI 304 austenitic stainless steel in simulated walking beam furnace conditions

Aleksi LAUKKA[1)], Eetu-Pekka HEIKKINEN[1)], Esa PUUKKO[2)] and Timo FABRITIUS[1)*]

M.sc (tech). Aleksi Laukka, D.sc (tech) Eetu-Pekka Heikkinen, Prof. Timo Fabritius

[1)] Process metallurgy research group, University of Oulu, Pentti Kaiteran katu 1, 90014, Oulu, Finland

E-mail: timo.fabritius@oulu.fi

Mr. Esa Puukko

[2)] Research centre, Outokumpu Stainless PLC, Terästie, 95400, Tornio, Finland

Keywords: microalloying, austenitic stainless steel, scaling, thermogravimetric, slab

Abstract

The effect of microalloying boron and titanium on AISI 304 austenitic stainless steel scale formation is studied. Thermogravimetric tests simulating walking beam furnace conditions are performed at temperatures of 800, 1100 and 1300 °C for three hours on samples of AISI 304 steels with different alloying amounts of B and Ti. Scaling at 800 °C is negligible on all the samples while scaling is clear at 1100 and 1300 °C. The thermogravimetric results show that even in small amounts, boron and titanium have an effect on scale growth rate. FESEM microscopy and accompanying EDS analyses are used to study oxidation area element composition. The FESEM images are also used to compare the oxidation zones' area fractions of metal, pores and oxide between different alloying amounts for the samples of 1300 °C tests. Calculations for scale formation activation energy are done based on the thermogravimetric data. The steel sample with the lowest alloying of boron and titanium shows a noticeably different growth rate, which is nearly linear in both the 1100 and 1300 °C tests. Differences between alloying amounts in accumulated scale during the 180-minute period in kg/m2 are greater at 1100 °C than they are at 1300 °C.

1. Introduction

Stainless steel slab reheating prior to hot rolling produces a scale layer on the surface of the slab. The composition, structure and amount of this scale layer depend on the composition of the steel. While the high temperature oxidation behaviour of austenitic stainless steel has been largely researched, the effects of microalloying elements on scaling has not been studied thoroughly.

Previous AISI 304 stainless steel scaling property research has focused on comparisons between different AISI standards such as AISI 303[1], AISI 304L[2], AISI 316[3, 4], AISI 430[5] and AISI 439 [6, 7] over short, lengthened or cyclic time periods. In this research, the effects of titanium and boron on AISI 304 scaling behaviour under simulated reheating furnace conditions has been investigated.

Operating reheating furnaces to take account of the scaling properties of individual slabs is important from the industry's perspective in order to minimize direct costs in terms of material loss in the form of scale, and indirect costs in the form of end product quality loss when descaling does not fully succeed.

The purpose of this research was to observe the scaling in a time period similar to the time it takes a slab to travel through a reheat furnace. Other isothermal scaling studies have been conducted either in a time-frame of under 90 minutes [5, 8, 9], or over ten hours [1, 2, 4, 6]. In this research, the time-frame was set to 180 minutes according to an industry partner's average evaluation of the time a slab is in the reheat furnace.

The operation of an industrial scale walking beam slab reheat furnace had shown that microalloying titanium could have a reducing effect to the scaling amount of AISI 304 stainless steel. It was also hypothesized that microalloying boron could have a reducing effect to scaling amount. These arguments led to the series of tests performed in this research with varying microalloying amounts of boron and titanium.

2. Methods

The stainless steel samples used in the experiments were prepared from the same AISI 304 slab's cut-off pieces and alloyed for the desired boron and titanium contents in a vacuum induction furnace. The cut-offs and alloying elements were melted in a small scale induction oven and cast into 300 x 450 x 50 mm slabs. The slabs were cut into halves and from the middle of the slab, a 1 cm cross section of the slab was utilized as the sample area. Out of this cross-section, a 1.7 cm wide piece was cut out and this piece was subsequently cut into a 3 cm tall piece. This bulk sample piece was then sliced into 2 mm thick loaves which were the finished test subjects. The sample preparation is clarified in parts (a) through (f) of **Figure 1**. In total, samples with four different alloying amounts of boron and titanium alloyed steel were prepared.

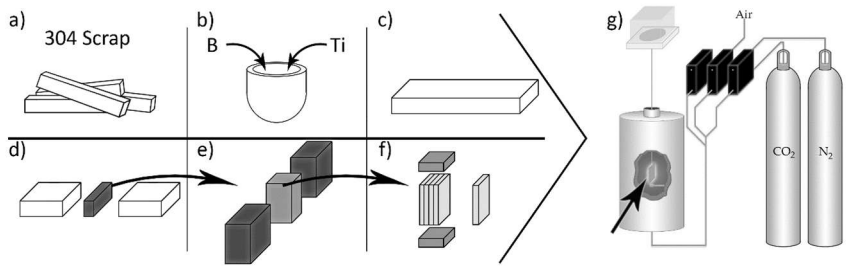

Figure 1. Slab cut-off evolution: a) scrap from AISI 304 slabs, b) melting of the scrap and addition of boron and/ or titanium, c) cast laboratory-scale slab, d) cut from a scrap cross-section (dark), e) cut of the sample bulk piece (grey) and f) cut of the final samples (light grey). The thermogravimetric (TG) oven setup is shown in g); the arrow points to the sample in the oven, black boxes are mass flow controllers. Schematic illustration.

The alloying amounts for boron and titanium are presented in **Table 1**, along with the area measured for the sample in question. Each sample was measured with a digital caliper from both ends for thickness, length and width and the average value was used for area calculation.

Table 1. Research matrix with sample composition for B and Ti along with temperature, time and the measured surface area of the samples.

Id	B (ppm)	Ti (ppm)	T (°C)	t (min)	Area (mm2)
1510L	7	<100 *	800	180	1241.64
1510L	7	<100 *	1100	180	1215.66
1510L	7	<100 *	1300	180	1255.99
1511L	7	400	800	180	1295.84
1511L	7	400	1100	180	1282.87
1511L	7	400	1300	180	1299.52
1512L	55	100	800	180	1300.84
1512L	55	100	1100	180	1220.64
1512L	55	100	1300	180	1246.63
1513L	35	100	800	180	1288.35
1513L	35	100	1100	180	1351.33
1513L	35	100	1300	180	1243.93

*Element's analysis lower limit was at 100ppm

The scaling behaviour was investigated by carrying out a thermogravimetric analysis. The samples were placed in a thermogravimetric oven with the sample strung by a platinum wire from a scale. Inside the oven, the temperature was either 800, 1100 or 1300 °C with the free oxygen amount fixed at 5 % to simulate the atmosphere in a walking beam furnace (76.19 % CO_2, 18.81 % N_2, 5 % O_2). The oxygen content was controlled by feeding CO_2, N_2 and pressurized air through mass flow controllers to the oven. The weighing scale, mass flow controllers and thermocouple were connected to a computer to allow real-time measurement of the sample weight, as well as the prevailing atmosphere and temperature. All the samples were

subjected to an isothermal atmosphere of either 800, 1100 or 1300 °C for 180 minutes. The used thermogravimetric oven setup is illustrated in step (g) of Figure 1.

Prior to oven insertion, the samples were cleaned with acetone and pickled clean of surface passive oxidation with a 2.5 % HCl solution. The samples were immersed in the solution for 39 seconds based on calculations with the assumption of the passive oxidation layer being 4 nm [10] thick for an AISI 304 stainless steel and the 2.5 % HCl solution having a corrosion rate of 25 $g/m^2 \cdot d$ [11] at room temperature and the passive oxide layer having a density of 5.71 g/cm^3 assuming that the passive oxide layer consists of 65 wt-% Cr+Cr oxide (25 wt-% Cr and 75 wt-% Cr_2O_3) and 35 wt-% Fe+Fe oxide (25 wt-% Fe and 75 wt-% Fe_3O_4)[12].

After the samples were removed from the thermogravimetric oven, they were allowed to cool down before being encased in epoxy. The epoxy covered sample was cut in half and polished for further field emission scanning electron microscope (FESEM) examination of the sample cross section. In the FESEM observation, energy dispersive spectroscopy (EDS) point analyses were carried out on the sample oxidation regions to determine the chemical composition the regions' sub-zones.

Based on the thermogravimetric data, the activation energies of the oxidation were calculated for the samples through an Arrhenius type equation. From the combined FESEM and EDS data, a per-oxidation area composition depth-chart of the oxide layer was formed for two samples at 1300 °C. Additionally, an oxidation area comparison was made for all samples at 1300 °C.

3. Results

The primary results gained from the thermogravimetric oven tests were the mass increases as a function of time. To compare results between samples, the mass increases were converted to the mass increase per pre-measured area of the sample. The area normalized thermogravimetric results are presented in **Figure 2** where the temperature is at (a) 800 °C, (b) 1100 °C, (c) 1300 °C and (d) 1300 °C for the first 15 minutes of the test.

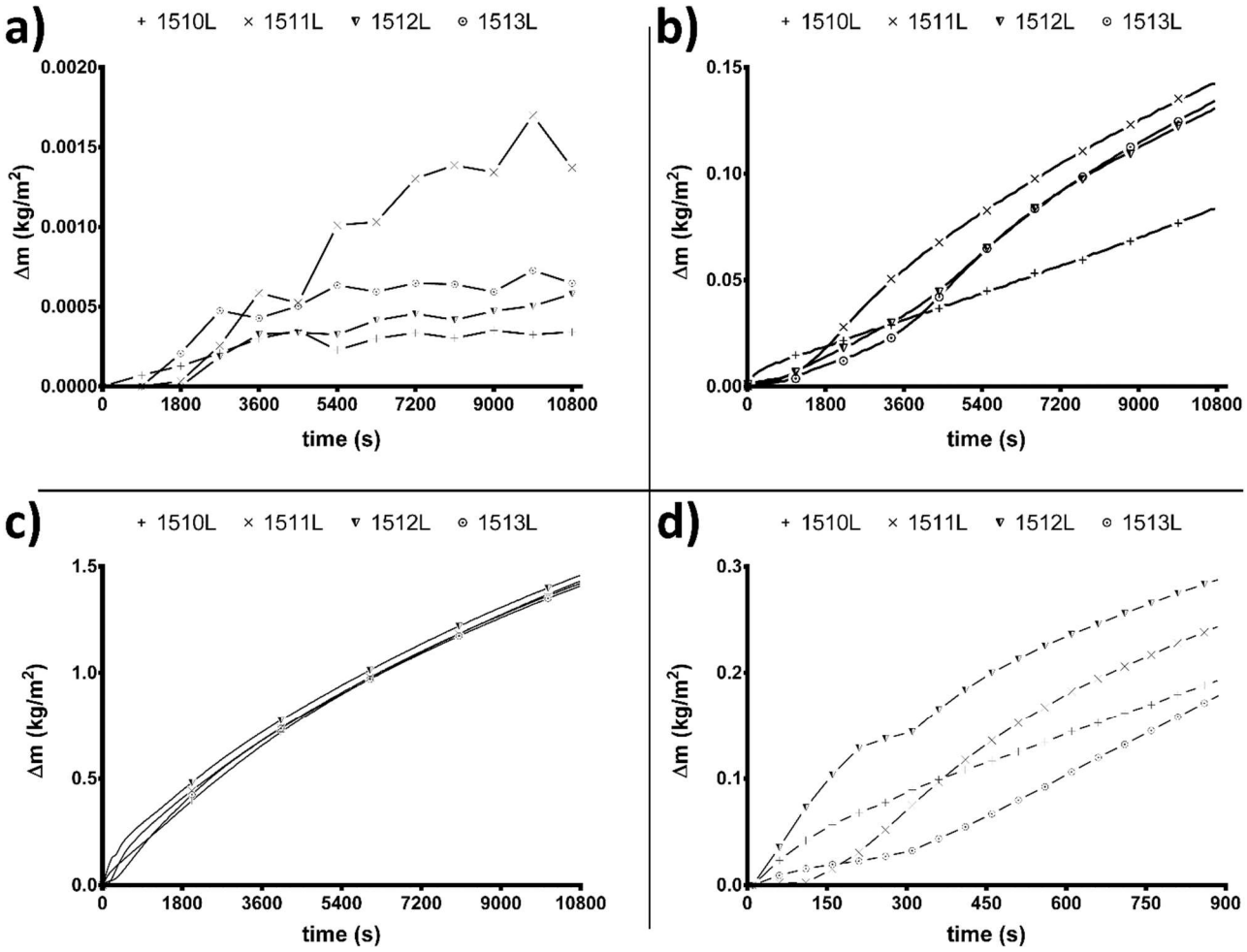

Figure 2. Scale growths at; a) 800 °C as 90 measurement averages, b) 1100 °C, c) 1300 °C and d) 1300 °C for the first 15 minutes.

FESEM inspection along with EDS analyses were performed on the samples at temperatures of 1100 °C and 1300 °C. The different oxidation zones at 1300 °C were of particular interest and the evolution of different oxides inside the zones was inspected as a function of depth from the surface. Additionally, the zones' relative area ratios were further analysed with the help of pixel-based calculation and image analysis. The overview pictures of the scale layer in each of the temperatures are presented in **Figure 3**. In the figure, (a) shows the overview in sample 1511L at 800 °C as observed through an optical microscope, whereas (b) and (d) show FESEM imagery of the 1100 °C test samples 1512L and 1513L respectively, and (c) and (e) show FESEM imagery of the 1300 °C test samples 1510L and 1513L respectively.

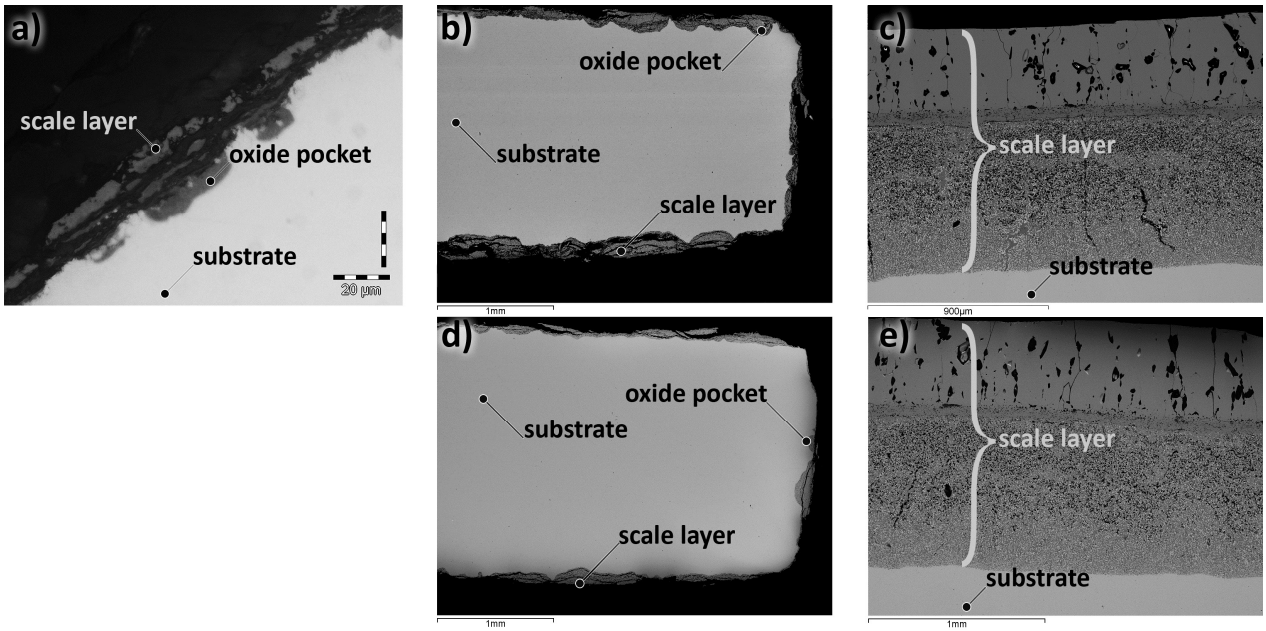

Figure 3. Comparison of the scale layers' thickness between different samples in different temperatures with the locations of the substrate steel, oxide pocket and scale layer; a) the optical microscope image of the sample 1511L after a TG oven test at 800 °C, FESEM images of samples 1512L (b) and 1513L (d) after a TG oven test at 1100 °C , and FESEM images of samples 1510L (c) and 1513L (e) after a TG oven test at 1300 °C.

3.1. Tests at 800 °C

Scaling occurring at the temperature of 800 °C was minimal. The unmodified test data suggested only measurement noise, but when the results were graphed as 90 measurement averages, some indication of oxidation was seen, as is displayed in part (a) of Figure 2. However, in comparison to scale formation at higher temperatures, this oxidation is considered negligible.

While all of the samples show some oxidation happening, sample 1511L stands out. The other samples show the oxidation levelling off after roughly 4000 seconds but 1511L continues to oxidize at a procedural rate.

The oxide growth at 800 °C was so scarce that out of the cross-sectioned samples intended for FESEM analysis, only 1511L had oxide pockets, as can be interpreted from the scale growth data in Figure 2, part (a). An optical microscope image of this sample and the oxide pocket is presented in part (a) of Figure 3.

3.2. Tests at 1100 °C

The progressive scale growth data at 1100 °C from the thermogravimetric oven is shown in part (b) of Figure 2. Three of the samples show clear breakaway oxidation happening after 2000 to 4000 seconds into the test. Sample 1510L, with low titanium and boron content, shows almost linear oxidation behaviour throughout the test. The specific scale growths are in order from highest to lowest: 1511L, 1513L, 1512L and 1510L.

Removing the samples from the oven's 1100 °C temperature resulted in the oxide layer partially coming off due to the uneven cooling properties of the scale layer and metal substrate.

The incoherent, brittle and thin oxide layer that formed at 1100 °C is presented in Figure 3, part (b) for the sample 1512L and part (d) for the sample 1513L. The layer shows a lamellar structure with alternating oxidation zones within the layer. All samples at 1100 °C showed similar layer properties and the blown out appearance is caused by some of the scales breaking loose upon oven removal.

3.3. Tests at 1300 °C

Scale formation rate of samples were very close to each other at 1300 °C and are presented in part (c) of Figure 2. The highest weight gain per area was for the low-Ti, high-B sample 1512L at 1.460 kg/m2, followed by the high-Ti, low-B sample 1511L at 1.44 kg/m^2. The second-lowest weight gain was for the sample low-Ti, low-B sample 1510L at and the lowest for the low-Ti, med-B sample 1513L at 1.409 kg/m^2. The difference between the highest and lowest amount of scaling is only 3.5 % at this temperature compared to the much higher 42 % difference between the highest and lowest scaling amounts at 1100 °C.

The difference between the samples was largest during the first 15 minutes. Part (d) of Figure 2 shows the scale growth lines for the first 15 minutes in the thermogravimetric oven at 1300 °C. From the figure, it can be seen that as in the 1100 °C tests, sample 1510L shows a scale growth curve which is different from the others. The curve does not indicate breakaway oxidation starting to happen later in the test but, rather, it occurs at the very beginning of the test. Another

interesting sample is 1512L which shows the same initially fast oxidation rate as 1510L with the difference of settling for a minute before speeding up again.

An overview of the thick, adherent oxide layer that formed at 1300 °C is presented in Figure 3, part (c) for the sample 1510L and part (e) for the sample 1513L. The layer exhibits a multi-layered structure with the whole layer being substantially thicker and more consistent than the layer formed at 1100 °C.

3.4. Activation energy analysis

The thermogravimetric data was transformed to a scale growth slope dm/dt which was combined with the partial pressure of oxygen to acquire the rate constant value for the Arrhenius equation presented in equation (1).

$$k = A \cdot e^{-\frac{E_A}{R \cdot T}} \cdot p_{O_2} \quad (1)$$

Equation (1) can be rewritten as equation (2) as:

$$\ln k = \ln\left(A \cdot p_{O_2}\right) - \frac{E_A}{R} \cdot \frac{1}{T} \quad (2)$$

which is a linear equation and can be plotted as an Arrhenius plot using ln(k) as a function of 1/T to determine the activation energy and pre-exponential factors. The Arrhenius plots for all of the samples are presented in **Figure 4**.

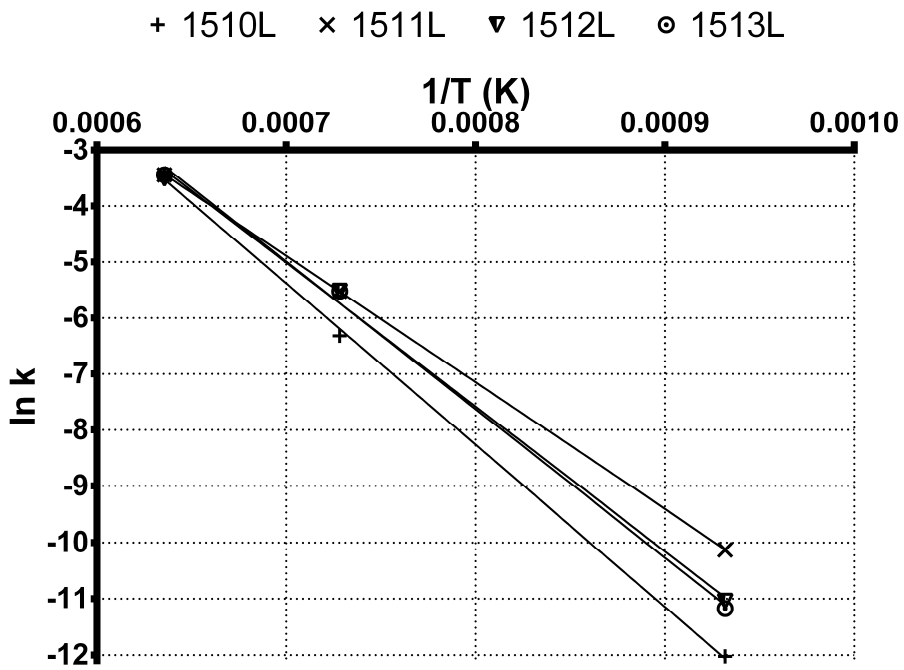

Figure 4. Arrhenius plots for sample oxidation constants.

The activation energies and pre-exponential factors for the samples are presented in **Table 2**. It is observed that the sample low-Ti, low-B sample 1510L has the highest activation energy and the high-Ti, low-B has the lowest activation energy. The activation energy values are in good accordance with other AISI 304 oxidation research, where values of 231 kJ/mol in air atmosphere [6], 239 kJ/mol in a pure oxygen atmosphere [6] and 226 kJ/mol in an air atmosphere with 3 ppm H_2O [5] have been acquired.

Table 2. Values for activation energies and pre-exponential factors calculated from the Arrhenius plot.

Sample	A $(1/s)\cdot 10^6$	Ea (kJ mol^{-1})
1510L	53.05	240
1511L	1.10	188
1512L	8.79	214
1513L	14.30	219

3.5. Microscopic analysis

As was seen in parts (b) and (d) of Figure 3, the oxidized areas of the cross-sectioned 1100 °C samples consisted of oxide pockets with a thin scale layer positioned above them. The scale layer included two areas; positioned outside the sample there was an iron oxide layer and positioned towards the sample centre, there was an oxide layer containing minor amounts of chromium, nickel, manganese and a major amount of iron.

The scale layer formed at 1100 °C is separated into three different zones, as presented in **Figure 5**, part (i). Zone (a) represents the substrate metal. Zone (b) is the inner oxidation layer containing pores, cracks likely due to the scale spallation, oxidized areas and metallic areas. Zone (c) is the differentiating oxidation zone separating the outer and inner oxidation zones and zone (d) is the outer oxidation zone containing only ferrous oxide.

The scale layer formed at 1300 °C is separated into four different zones, as presented in Figure 5, part (ii). The 0-zone represents the substrate metal. Zone I is the pore-free inner oxidation zone. Zone II is the porous intermediate oxidation zone. Zone III is the differentiating oxidation zone containing no metallic areas and zone IV is the outer oxidation zone consisting of ferrous oxide. For the area calculations, the inner oxidation zone was determined to end 200 μm after it started and the intermediate layer to end where the metal containing areas ended.

It is probable that the zones from 1100 °C are an intermediate step to the evolution of the zones at 1300 °C at some time during the experiment. Specifically, in a way that zone (b) is an intermediate step to the evolution of zones I and II, zone (c) gets refined to zone III and zone (d) grows outwards to zone IV.

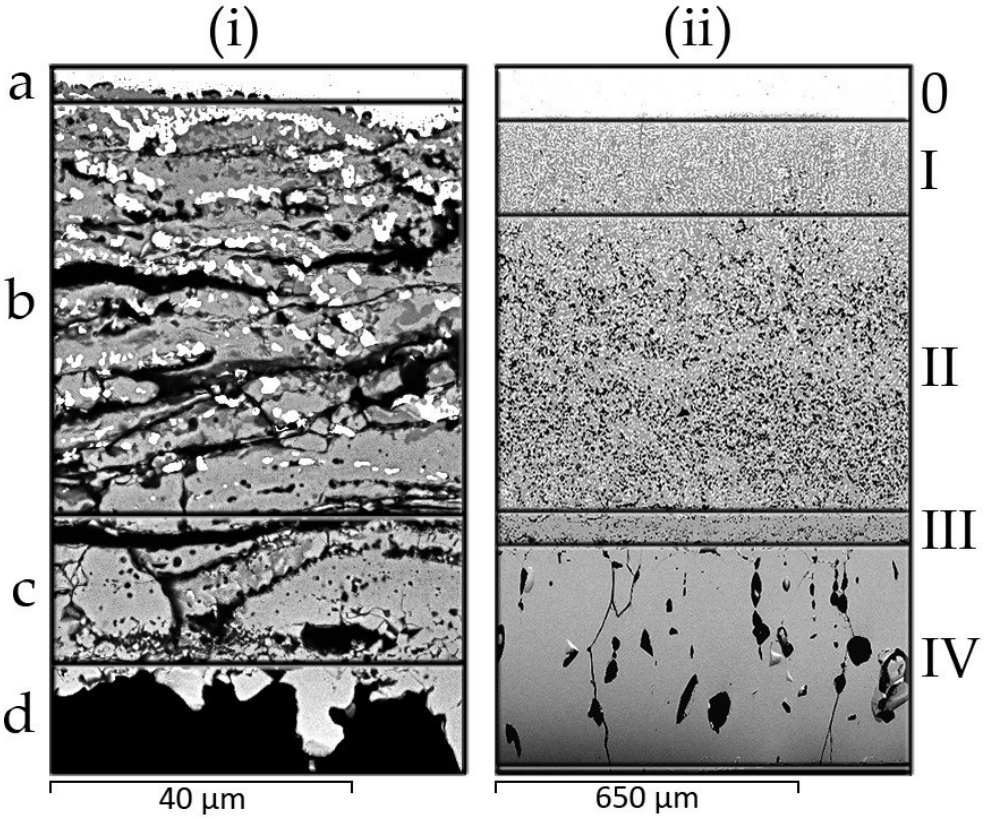

Figure 5. Oxidation zones formed at 1100 °C (i), taken from the sample 1512L: (a) substrate metal, (b) inner oxidation zone, (c) differentiating oxidation zone and (d) outer oxidation zone. At 1300 °C (ii), taken from the sample 1513L: (0) substrate metal, (I) inner oxidation zone, (II) intermediate oxidation zone, (III) differentiating oxidation zone and (IV) outer oxidation zone.

For the samples 1511L and 1513L, EDS analysis point (AP) locations from the 1300 °C tests are shown in **Figure 6** and the chemical composition analyses for them are presented in **Table 3**. The inner and intermediate oxidation zones of the 1300 °C samples contained three distinct oxidized areas and the metallic area. The metallic area can be found at analysis points 4, 10, 13, 17, 19, 24, 26 and 30 through 35, showing nickel enrichment and chrome depletion. The oxide areas were iron-rich oxide (AP 1, 7, 9, 18, 20, 28 and 29), chrome-iron oxide (AP 2, 3, 5, 6, 8, 12, 15, 16, 21-23, 25 and 27) and silicon-iron oxide (AP 11 and 14).

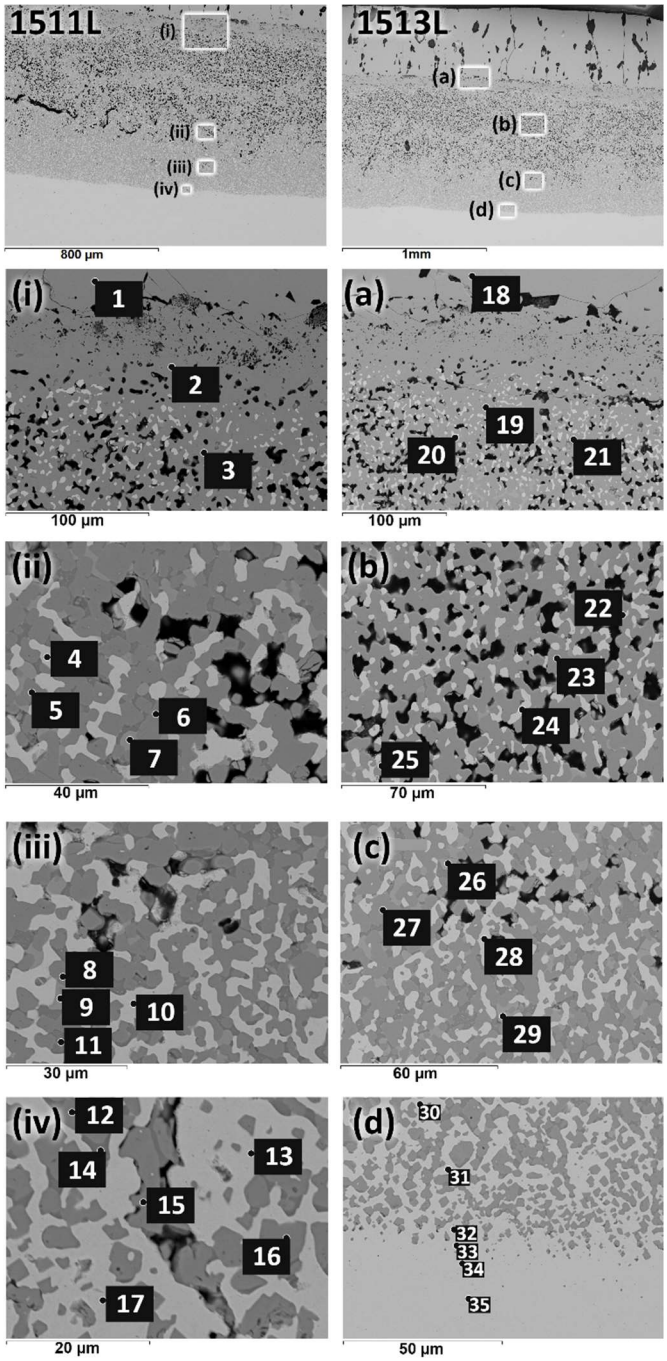

Figure 6. The scale layer analysis point locations of the samples 1511L (left; i, ii, iii and iv) and 1513L (right; a, b, c and d) for tests performed at 1300 °C. Images (i) and (a) are from the intermediate oxidation zone, images (ii) and (b) are from the intermediate oxidation zone, images (iii) and (c) are from the inner oxidation zone and images (iv) and (d) are from the boundary of the steel substrate and inner oxidation layer.

Table 3. 1300 °C analysis point compositions of samples 1511L and 1513L in wt-%, analysis point origins are denoted in Figure 6.

Analysis point	O	Si	P	Cr	Mn	Fe	Ni
AP 1	25.05			3.57	1.75	66.08	1.56
AP 2	26.22			28.12	1.34	43.47	0.68
AP 3	26.02			32.44	1.27	38.24	
AP 4				2.97		72.13	24.68
AP 5	26.44			36.42	1.62	34.33	
AP 6	26.61			38.22	1.66	32.76	
AP 7	21.21	0.32		4.08	0.75	73.91	
AP 8	26.74			40.18	1.20	31.05	
AP 9	21.69	0.30		3.82	0.99	72.66	
AP 10				3.06		79.58	17.99
AP 11	27.56	11.86	0.78	2.03	2.51	55.46	
AP 12	27.06			46.02	2.98	24.35	
AP 13				2.91		85.15	12.38
AP 14	28.97	13.37	0.66	1.72	2.49	52.80	
AP 15	26.58			42.27	1.50	28.06	
AP 16	27.32			46.11	4.14	22.97	
AP 17				2.52		89.20	9.64
AP 18	24.06			1.72	1.54	67.29	1.70
AP 19				2.93		41.68	53.99
AP 20	18.20	0.29		4.25	0.87	71.31	1.33
AP 21	25.25			31.83	1.81	38.63	
AP 22	26.27			33.60	1.70	36.80	
AP 23	25.54			34.52	1.51	36.39	
AP 24				2.93		56.01	38.60
AP 25	24.75			23.64	1.33	48.22	
AP 26				3.00		74.82	20.90
AP 27	26.15			38.48	1.23	34.17	
AP 28	21.17	0.35		3.57	0.95	73.04	
AP 29	21.44	0.30		3.88	1.12	72.61	
AP 30				2.85		82.25	15.55
AP 31				2.72		84.51	14.22
AP 32				2.88		86.22	11.69
AP 33				10.86		80.28	8.96
AP 34		0.51		18.32	1.40	71.66	8.50
AP 35		0.60		19.14	1.67	71.17	8.04

One curiosity is the tendency of phosphorous to be found at high quantities in the silicon-iron oxide area. The alloyed phosphorous was 300 ppm whereas in the silicon-iron oxide area, the

content of phosphorous was around 7000 ppm, as shown in AP 11 and 14. The nickel enrichment and iron depletion in the metallic area was proportional to the depth from the substrate surface up until to the start of outer oxidation zone. Chromium depletion was very abrupt and decreased from around 20 % in the substrate to around 3 % in a length of 20 µm when going into the inner oxidation zone, as is shown from analysis points 30 through 35 in Table 4. Nickel content in the metallic area increased to almost 54 wt-% at the edge of the intermediate oxidation zone. Non-oxide areas cease to exist past the intermediate oxidation zone. The metallic area's nickel, chrome and iron content depth profile of sample 1513L at 1300 °C is presented in **Figure 7**. Markers in the FESEM image represent individual EDS point analyses.

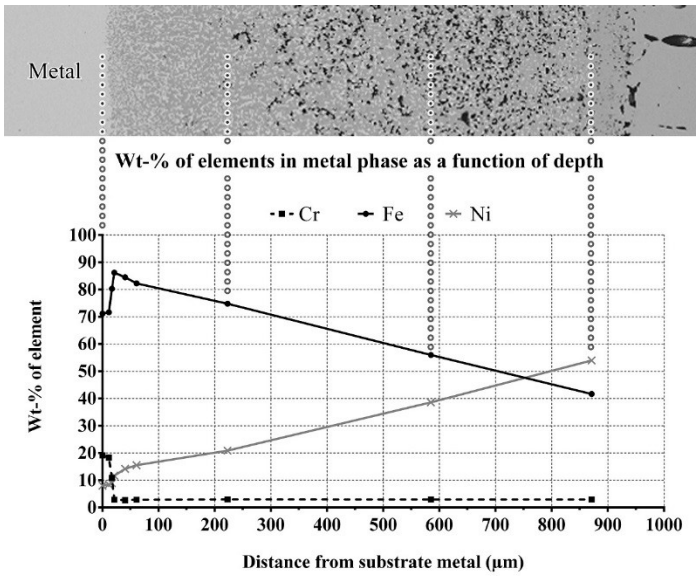

Figure 7. Metallic area composition depth chart of the sample 1513L at 1300 °C.

3.6. Oxidation layer sub-zone analysis

The area fractions of the oxide, metal and porous zones throughout the scale layer were determined from the FESEM images. This was done with the help of an image analysis in which

the pixel count of each zone's sub-areas, i.e. the pore, metal and oxide areas, was compared to the total pixel count of the oxidation zone. A calculation was performed for three images taken from different location in the sample for each of the 1300 °C samples and the averaged results are presented in **Table 4**.

Table 4. Oxidation layer area fractions for tests at 1300 °C.

Inner oxidation zone(I)			
Sample	Pores (%)	Metal (%)	Oxide (%)
1510L (low-Ti, low-B)	1.21	20.76	78.03
1511L (high-Ti, low-B)	0.09	45.72	54.19
1512L (low-Ti, high-B)	0.18	40.44	59.39
1513L (low-Ti, med-B)	0.36	23.66	75.98
Intermediate oxidation zone(II)			
Sample	Pores (%)	Metal (%)	Oxide (%)
1510L (low-Ti, low-B)	17.04	23.00	59.96
1511L (high-Ti, low-B)	15.08	23.97	60.95
1512L (low-Ti, high-B)	14.57	24.67	60.76
1513L (low-Ti, med-B)	10.14	21.82	68.04

The clearest differences in the inner oxidation zone area fractions can be seen between two groups of samples: 1510L and 1513L versus 1511L and 1512L. The low boron, low titanium alloyed sample 1510L and the medium boron, low titanium sample 1513L, have higher oxide and porous area fractions when compared to the other two samples.

In the intermediate oxidation zone, the differences are more minor with sample 1510L having the lowest oxide area fraction and sample 1513L having the highest. Interestingly they are the opposites at pore fraction as well. The sample 1510L has the highest amounts of pores in the layer and 1513L has the least amount of pores. The area fractions for the samples 1511L and 1512L are nearly identical.

4. Discussion

Boron and titanium microalloying caused the scale layer morphology to differ between samples. More specifically at 1300 °C, the inner and intermediate oxidation layers' sub-area fractions of pores, metal and oxides varied greatly. The largest differences were found between the inner oxidation zone metallic area compositions of the low to medium boron additions and the high boron addition. Based on previous study regarding scale entanglement with the metal substrate, it was observed that the presence of metal-free fracture paths throughout the scale layer is favourable to descaling [13] and the presence of oxide "pegs" protruding into the metal substrate at the scale-metal substrate interface is detrimental to descaling, especially in alloys containing Ni and Si [13–15]. Based on these results, the more metal-free zones there are in the inner and intermediate oxidation zones, the easier it is to remove the scale layer. As such, the low-boron, low-titanium sample 1510L fills this requirement the best.

When compared to the AISI 304 alloyed with 7 ppm boron, higher boron alloying of 35 and 55 ppm caused the activation energies of these alloys to decrease. Also viewing the first fifteen minutes of the TG data at 1300 °C shows that microalloying boron leads to the oxidation happening more rapidly in the beginning of the test while becoming harder towards the end while with the low boron microalloying, oxidation rate is more or less the same throughout. Taking further into account that sample 1510L has the highest activation energy, and from the view of scale formation and speculatively the scale layer's removal, it is not favourable to micro-alloy titanium between 100 and 400 ppm to AISI 304 austenitic stainless steel. Micro-alloying boron seems beneficial up to 35 ppm, as the sample 1513L had the lowest scaling per area at 1300 °C, which is near the maximum temperatures reached in a reheat furnace.

It should be noted that these studies were performed in an atmosphere containing 5 % free oxygen but without H_2O. Other research suggests that adding water vapour to otherwise dry air causes the oxidation rate to increase and to increase the amount of pores in the formed scale layer [16].

The results gathered in this research show that boron microalloying to AISI 304 leads to different growth rates in any one temperature at a given time and the accumulated scale amount. It is therefore hypothesized that boron microalloying affects the growth speed and or order of growth of the scale layer and its sub-zones through a mechanism not exactly shown by these tests alone. The scale layer's area fractions at 1300 °C would indicate that the formation of the oxide areas versus the contraction of metallic areas in the inner oxide layer and the formation of pores in the intermediate oxide layer play a key role in the growth order of the whole scale layer.

What comes from the microalloying of titanium to the scale formation is a bit of surprise. It was assumed that microalloying titanium would have a reducing effect to the scale formation amount of AISI 304 in walking beam furnace conditions. The performed tests show that the sample with the highest alloying amount of titanium at 400 ppm (1511L) had highest accumulated scaling amounts at 800 °C and 1100 °C while having the second lowest accumulated scaling amount at 1300 °C. It could very well be that titanium microalloying did better in the region between 1100 °C and 1300 °C in both scaling amount and scale growth rate.

Placing emphasis on the time period and the oxygen content to those used in a walking beam furnace before hot rolling, these results can be used to tune the operation of the furnace. The

results show boron and titanium microalloying affects the scale formation amount and scale layer morphology. Performing research on the effects of microalloying elements' effect on scale formation for high volume steel types such as the AISI 304 can be seen beneficial from both a direct and an indirect financial standpoint. The direct financial effect is mitigated material loss to scaling while the indirect effect comes from reduced end product quality issues related to insufficient scale removal prior to hot rolling. Even further, doing standardized tests on a select group of microalloying elements for several steel types can lead to an estimation model to provide preliminary scaling results on untested steels.

Further research to acquire the specific temperature where the scale layer adheres to the substrate metal and the cause behind this is planned along with the effects caused by adding water vapour to the atmosphere.

5. Conclusion

The aim of the research was to study the effect of boron and titanium microalloying on scale formation for AISI 304 austenitic stainless steel in simulated walking beam furnace conditions. Boron and titanium micro-alloying had observable effects on scaling:

-Thermogravimetric results show clear differences, depending on the B and Ti content in accumulated scale amounts at 1100 °C temperature and slight differences at 1300 °C

-The low boron, low titanium sample had the highest activation energy for oxidation while the high titanium, low boron had the lowest activation energy

-The formed scale layer at 1300 °C has a distinct morphology; the area fractions of pores, metal and oxide of the inner and intermediate oxidation zones differed greatly between samples

-Solely from the view of scale formation, microalloying titanium between 100 and 400 ppm is not beneficial, while alloying boron is beneficial up to 35 ppm

-Boron microalloying affects the scale layer growth rate and accumulated scale amount through an intricate mechanism not fully revealed through the performed tests but is tied to the formation of oxide areas and pores, and contraction of metallic areas in the inner and intermediate oxidation zones

6. Acknowledgements

This research has been conducted within the FIMECC SIMP, a research program coordinated by the Finnish Metals and Engineering Competence Cluster (FIMECC). Outokumpu Stainless is acknowledged for funding and for their committed collaboration. In particular the authors would like to thank the Research Centre of Outokumpu Tornio for manufacturing the samples and the laboratory staff of the process metallurgy research group at the University of Oulu for practical guidance on sample handling.

Received: ((will be filled in by the editorial staff))

Revised: ((will be filled in by the editorial staff))

Published online: ((will be filled in by the editorial staff))

References

[1] E. Fedorova, M. Braccini, V. Parry, C. Pascal, M. Mantel, F. Roussel-Dherbey, D. Oquab, Y. Wouters, and D. Monceau, Corros. Sci., **2016**, 103, 145.

[2] A. Col, V. Parry, and C. Pascal, Corros. Sci., **2016**, 114, 17.

[3] R. Guillamet, J. Lopitaux, B. Hannoyer, and M. Lenglet, *J.Phys.IV Fr.*, **1993**, 3,349.

[4] K. a. Habib, M. S. Damra, J. J. Saura, I. Cervera, and J. Bellés, *Int. J. Corros.*, **2011**, 2011, 1.

[5] C. E. R. Carvalho, G. M. Costa, A. B. Cota, and E. H. Rossi, *Mater. Res.*, **2006**, 9, 393.

[6] A. M. Huntz, A. Reckmann, C. Haut, C. Sévérac, M. Herbst, F. C. T. Resende, and A. C. S. Sabioni, *Mater. Sci. Eng. A*, **2007**, 447, 266.

[7] A. Sabioni, A.-M. Huntz, E. Conceição da Luz, M. Mantel, and C. Haut, *Mater. Res.*, **2003**, 6, 179.

[8] B. Ozturk and R. Matway, *ISIJ Int.*, **1997,** 37, 169.

[9] T. Kizu, Y. Nagataki, T. Inazumi, and Y. Hosoya, *ISIJ Int.*, **2002**, 42, 206.

[10] G. Lorang, M. Da Cunha Belo, A. M. P. Simões, and M. G. S. Ferreira, *J. Electrochem. Soc.*, **1994**, 141, 3347.

[11] A. J. Sedriks, *Corrosion of stainless steels*, John Wiley, New York **1979**, 222.

[12] G. Henkel and B. Henkel, *Information on passivation layer phenomena for austenitic stainless steel alloys,* Henkel-EPOL, **2003**, 2, Technical report.

[13] P. C. Pistorius, *J. S. Afr. Inst. Min. Metall.*, **2003**, 103, 607.

[14] W. Melfo, H. Bolt, M. Rijnders, D. Staalman, C. B. Castro, D. Crowther, and B. Jana, *ISIJ Int.*, **2013**, 53, 866.

[15] J.-J. N. Mukadi and P. C. Pistorius, *Ironmak. Steelmak.*, **2010**, 37, 57.

[16] S. R. J. Saunders, M. Monteiro, and F. Rizzo, *Prog. Mater. Sci.*, **2008**, 53, 775.

Table of contents entry

In a thermogravimetric oven, simulated walking beam furnace conditions are used to study the effect boron and titanium microalloying have on the forming scale layer's growth and morphology of AISI 304 austenitic stainless steel. Results include area normalized scale growth graphs with further analysis done through FESEM microscopy, EDS analysis and activation energy calculation.

Aleksi LAUKKA, Eetu-Pekka HEIKKINEN, Esa PUUKKO and Timo FABRITIUS

The effect of boron and titanium microalloying on the scale formation of AISI 304 austenitic stainless steel in simulated walking beam furnace conditions

ToC Figure